Nonlinear Optical Spectroscopic Studies of Energy Transfer in Phospholipid Bilayer Liposomes Embedded with Porphyrin Sensitizers

Darius Kuciauskas,*,† Christopher J. Wohl,† Mark Pouy,† Aquelah Nasai,† and Vidmantas Gulbinas‡

Department of Chemistry, Virginia Commonwealth University, Richmond, Virginia 23284-2006, and Institute of Physics, Vilnius, Lithuania

Received: February 2, 2004; In Final Form: July 13, 2004

Transient grating kinetics were measured at different temperatures (1−40 °C) for DMPC phospholipid bilayer liposome aqueous dispersions. 5,10,15,20-Tetrakis-(4-hydroxyphenyl)-21,23H-porphyrin sensitizers were embedded into the phospholipid bilayers. Fluorescence emission temperature-dependence and quenching studies were used to determine that hydroxyphenyl porphyrins are localized in the aliphatic region of the phospholipid bilayer. Porphyrin localization does not change in gel (L_β') and liquid (L_α) phases of the membrane. In the transient grating experiment, following excitation with 100 fs 410 nm pulses, temperature and density modulations were observed as acoustic grating signals. Grating signal amplitude and the time when the acoustic peak reaches maximum were temperature-dependent. Negative time delay of the acoustic peak maximum was observed and explained by considering two thermal processes: (1) energy transfer from porphyrin to the phospholipid bilayer (described by a rate constant k_1), and (2) energy transfer from the phospholipid bilayer to the surrounding solvent (described by a rate constant k_2). A model accounting for time-dependent thermal expansion of phospholipid bilayers and water was developed to determine rate constants k_1 and k_2. The rate constant k_1 equals 7.14×10^{10} s^{-1} ($k_1^{-1} = 14$ ps) and is temperature-independent at 10−35 °C. The value of k_2 increases from 3.33×10^{10} s^{-1} ($k_2^{-1} = 30$ ps) at 10 °C to 5.56×10^{10} s^{-1} ($k_2^{-1} = 18$ ps) at 35 °C. The value and temperature dependence of k_2 suggest that thermalization in DMPC membrane occurs by thermal diffusion and vibrational energy transfer, but other phospholipid degrees of freedom (such as isomerization) are not involved in this process.

Introduction

Phospholipid bilayer vesicles (liposomes) are good cell membrane models and are widely used to study physical properties of biological membranes. Spectroscopic investigations of liposomes usually rely on membrane-embedded fluorescent or spin molecular probes; properties of such probes indirectly reflect properties of the phospholipid bilayer.[1] Likewise, liposomes are self-organized nanoscale molecular assemblies that have become increasingly important in molecular photonics and artificial photosynthesis. The function of such structures (for example, energy storage or signal transduction) can be controlled by light. This is achieved by using membrane-embedded molecular sensitizers.[2] Due to their large extinction coefficients and favorable redox properties, porphyrins are often used in membrane-based artificial assemblies.[3] Understanding porphyrin interactions with membranes is also important in photodynamic cancer therapy.[4]

All applications described above depend on energy transfer in liposome−sensitizer molecular assemblies. While thermal processes in solids are well understood and molecular vibrational relaxation is also widely studied, thermal processes in nanoscale structures have not been investigated thoroughly. The well-defined structure and narrow size distribution of liposomes make them well-suited for such studies. We examined thermal processes in 50-nm-diameter liposomes. We consider energy transfer from porphyrin molecular sensitizers to the phospholipid bilayer and from the bilayer to water. The system is also interesting because phospholipid bilayers undergo phase transitions from an ordered solid (gel) phase to a liquid phase. This phenomenon is sometimes associated with membrane functions in biological systems. The role the gel−liquid phase transition has on phospholipid bilayer properties (thermal relaxation and solvation) can be determined by studying thermal processes in each membrane phase.

We examined phospholipid bilayer liposomes with embedded 5,10,15,20-tetrakis-(4-hydroxyphenyl)-21,23H-porphyrins **1** and **2** (Scheme 1). Free-base hydroxyphenyl porphyrins sensitize singlet oxygen[5,6] and have been used in photodynamic cancer therapy.[7] Previous work has shown that porphyrin localization in phospholipid bilayers is not influenced by the central metal atom,[13] but rather, depends critically on macrocycle substitution.[8−12] Therefore, lipophilic (not soluble in water) free-base (H_2) porphyrin **1**, which shows strong fluorescence, was used to determine porphyrin localization in the phospholipid bilayers. Nonfluorescent Fe(III)Cl hydroxyphenyl porphyrins **2** were used in nonlinear optical experiments. Shorter porphyrin **2** excited-state lifetimes afforded picosecond time resolution in transient grating studies. Energy transfer in phospholipid bilayers (excited porphyrin → phospholipid bilayer → water) was compared with direct energy transfer from porphyrins to water. Direct energy transfer from porphyrin to water was studied using the water-soluble Fe(III) tetra-(*N*-methyl-4-pyridinium) porphyrin **3**.

* To whom correspondence should be addressed. E-mail: dkuciauskas@vcu.edu.
† Virginia Commonwealth University.
‡ Institute of Physics.

10.1021/jp049537f CCC: $27.50
Published on Web 09/04/2004

SCHEME 1

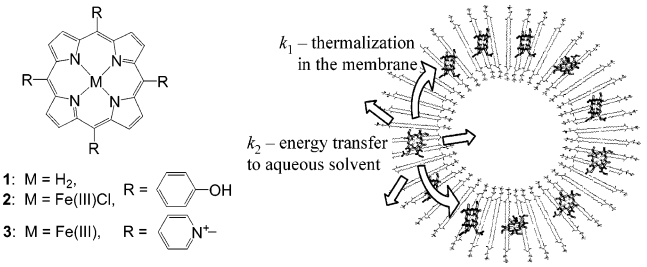

Energy transfer between molecules and the surrounding solvent has been examined by various spectroscopic techniques, including fluorescence line shape analysis, transient absorption, and Raman scattering. Transient grating spectroscopy has been used to study thermal processes for molecules in solution, films, and in heme proteins.[14−16] We applied transient grating spectroscopy to study porphyrin excited-state relaxation and vibrational energy transfer in phospholipid bilayer membranes and in aqueous solution.

Methods

In the transient grating experiment, two excitation pulses reach the sample at the same time (Scheme 2). Because of the excitation beam interference, light intensity is modulated along the coordinate x. If the light intensity is sufficiently high, nonlinear interactions lead to absorbance and/or refractive index modulation along x, creating a transient diffraction grating. In the case of resonant excitation, grating properties are largely determined by the changes in the absorption spectra and the corresponding modulation of the refractive index. After nonradiative relaxation of the electronic excited states, the grating is still present because of sample heating, dT, and density changes, $d\rho$. The modulation of the refractive index along the coordinate x may be described by a sine function: $\Delta n = \Delta n_{max}\sin(2\pi x/\Lambda)$. The grating period, Λ, depends on the angle between excitation beams, Θ, and on the excitation wavelength, λ: $\Lambda = \lambda/[2\sin(\Theta/2)]$. The probe pulse (which reaches the sample at a variable delay after the excitation pulses) is diffracted from the grating. Intensity of the diffracted signal, $I_{grating}$, under weak diffraction conditions is given by

$$I_{grating} \propto [\Delta n(t)]^2 = \left[\left(\frac{\partial n}{\partial T}\right)_\rho dT + \left(\frac{\partial n}{\partial \rho}\right)_T d\rho\right]^2 \qquad (1)$$

In this expression, the $(\partial n/\partial T)_\rho dT$ term represents heating, and the $(\partial n/\partial \rho)_T d\rho$ term represents density change due to the thermal expansion. The expression for $I_{grating}$ could also have terms related to absorption modulation.[16] dT and $d\rho$ are time-dependent, therefore, by measuring kinetics of the diffracted signal, dynamic properties of the transient grating can be investigated. Since the experiment relies on measurement of Δn, systems under study do not have to be fluorescent or have other "spectroscopic signatures" required for linear spectroscopy. An important advantage of the transient grating experiment is sensitivity—it is a zero background technique.

The $(\partial n/\partial T)_\rho dT$ and $(\partial n/\partial \rho)_T d\rho$ terms have different kinetics. The first term describes heat transfer from the solute to the medium and heat diffusion in the medium. In our experiments this term is much smaller (arguments for this statement are presented in Discussion), therefore we neglect it. The second term describes thermal expansion of the medium. Such expansion occurs with the speed of sound and evolution of the system may be described by a standing wave model. Experimentally, standing waves of density changes are observed as oscillations in the diffracted light intensity (Scheme 2). In the case of instantaneous solute excited-state relaxation and instantaneous heat transfer from solute to solvent, a sinusoidal transient grating signal would be observed

$$I_{grating} \propto A[\sin(wt)]^2 = A\left(\sin\frac{2\pi t}{\Pi}\right)^2$$

(where A is amplitude, w is frequency, $\Pi = 2\pi/w$ is period, and t is time) This case is illustrated as a dotted line in Scheme 2. If the excited-state relaxation and energy transfer to the solvent is not instantaneous but occurs with a finite rate, the phase of the acoustic wave, ϕ, will be different. The signal will then be described as

$$I_{grating} \propto A[\sin(wt + \phi)]^2 = A\left(\sin\frac{2\pi(t - t_c)}{\Pi}\right)^2$$

(where t_c is an acoustic peak delay). This case is illustrated with a solid line in Scheme 2. Therefore, the time when the first acoustic peak reaches its maximum, $t_{max} = \Pi/2 + t_c$, depends on the energy transfer rate.

Terazima and co-workers have studied several dyes in organic solvents and shown that t_c is equal to the thermalization time.[17,18] Therefore, by determining t_c values, rate constants for energy transfer from the solutes to the surrounding solvent can be obtained. Acoustic peak delays have also been analyzed in biological systems. Miyata and Terazima have recently observed negative t_c values for deoxymyoglobin aqueous solution.[19] By modeling transient grating data, these

SCHEME 2

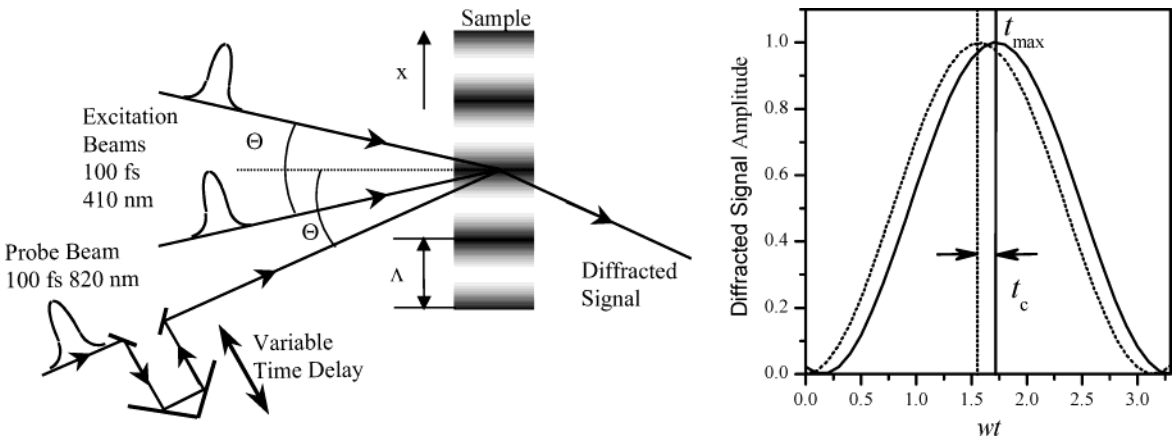

authors determined that 17% of the heme excess energy was transferred to water directly, while the majority of the heme energy was transferred to the protein.[19] By analyzing acoustic peak delay, Miller and co-workers studied picosecond conformational changes in carboxymyoglobin after ligand photolysis.[20]

The amplitude of the transient grating signal, *A*, is also an important parameter due to its temperature dependence. The amplitude of the acoustic signal in aqueous solution should be negligible at 4 °C, when the water thermal expansion coefficient is zero, and be amplified at higher temperatures. Temperature dependence measurements were successfully applied in transient grating studies of heme proteins and dye molecules.[14,21,22] As will be discussed below, the temperature dependence of the transient grating signal for liposome aqueous dispersion can be described by a simple model.

Experimental Section

Materials. 1,2-Dimyristoyl-*sn*-glycero-3-phosphocholine (DMPC) and 1,2-dipalmitoyl-*sn*-glycero-3-phosphocholine (DPPC) were obtained from Avanti Polar Lipids (10 mg/mL solutions in chloroform). Porphyrins **1** and **2** were obtained from Porphyrin Systems (Germany), and porphyrin **3** was purchased from Sigma. All other reagents and solvents were obtained from Aldrich.

Liposome Preparation. Sensitized liposomes were prepared by adding porphyrins dissolved in an organic solvent to DMPC or DPPC lipid solutions in chloroform. The solvent was then removed under an N_2 stream. The flask was placed in a warm-water bath (with the temperature above the phospholipid main phase transition) and phospholipids were hydrated with a phosphate buffer (50 mM, pH 7) to the final phospholipid concentration of 7.4 mM. This aqueous solution was then agitated with a low-power (10 W) ultrasonic bath until homogeneous in appearance, and extruded 11 times through a polycarbonate filter (50-nm pore diameter) while maintaining the temperature above the main phospholipid phase transition. Such preparation yielded unilamellar liposomes with a narrow size distribution and an average liposome diameter of 50 nm. The lipid-to-porphyrin ratio was varied from 100:1 to 1000:1 for fluorescence experiments and for transient grating experiments was 100:1. Liposomes without porphyrins were prepared following the same procedure. Nano-differential scanning calorimeter DSC II (Calorimetry Sciences Corporation) was used to obtain heat capacity profiles. Within experimental accuracy, heat capacity profiles were the same for 100:1 porphyrin sensitized concentration liposomes and for liposomes without porphyrins; both were similar to DSC data reported in the literature.[23] Electronic absorption spectra were measured with a HP8452A spectrometer and corrected for scattering. Fluorescence spectra were acquired with a Varian Eclipse fluorimeter equipped with a temperature controller.

Nonlinear Spectroscopy. The spectrometer for ultrafast nonlinear experiments was described previously;[24] it was modified for transient grating studies. A regeneratively amplified Ti:Sapphire laser system (Spectra Physics) provided 100 fs, 0.8 mJ pulses at 820 nm. The laser beam was split into two excitation beams (second harmonics generation in a 0.5-mm thick BBO crystal was used to obtain excitation pulses at 410 nm) and a probe beam (820 nm). The energies of the excitation and probe pulses were 2 μJ and 1 μJ, respectively. All beams were p-polarized. The grating period was $\Lambda = 1.73$ μm ($\Theta = 13.6°$ and $\lambda = 410$ nm). The probe beam was aligned to satisfy the phase matching conditions (the angle between the grating normal and the probe beam was equal to 13.6°, Scheme 2). Excitation beams were aligned in the horizontal plane, while the probe beam was offset from the horizontal plane by a small angle (~3°) to achieve better separation of the diffracted signal from the scattered light. Two iris diaphragms placed in the optical path of the signal beam reduced scattered probe light. A red filter was used to eliminate scattered excitation light. The diffracted signal was detected with a PMT (photosensor module H6780-20, Hamamatsu). The signal was amplified with a 300-MHz bandwidth amplifier (SR445, Stanford Research Systems) and was gated by a boxcar (SR250, Stanford Research Systems). A computer-controlled linear translation stage allowed adjustment of the probe beam time delay necessary to measure kinetics on the 100 fs to 3 ns time scale. Samples were placed in 2-mm path length cuvettes and stirred with a small magnet. Porphyrin absorption at 410 nm was approximately 0.65 for all experiments. Temperature was adjusted with a high-sensitivity thermostat (Flash 200, Quantum Northwest).

Results

Fluorescence Properties of Liposomes with Hydroxyphenyl Porphyrins Embedded in the Phospholipid Bilayer. Electronic absorption spectra of **1** and **2** and fluorescence emission spectrum of **1** are shown in Figure 1A. Porphyrin spectra are very similar in organic solvents and in phospholipid bilayers. For example, absorption band maxima for **1** are at 419 (Soret band), 516, 554, 594, and 650 nm (Q-bands) in acetone solution and at 423, 519, 557, 596, and 651 nm in liposomes. Porphyrin **1** is highly emissive in organic solvents (fluorescence emission quantum yield in acetone is 0.13,[5,6] emission maxima are at 657 and 723 nm). Emission maxima for **1**/DMPC liposomes are at 660 and 720 nm. Absorption maxima for porphyrin **2** in acetone solution are at 422, 512, 571 (shoulder), and 699 nm. For **2**/DMPC liposomes, the Soret band maximum is at 423 nm and the other weaker absorption bands are broadened.

Depending on the temperature, phospholipid membranes have very different structure and thermodynamic properties. Three major phases of phosphatidylcholine bilayers are the gel phase ($L_{\beta'}$), the rippled gel phase ($P_{\beta'}$), and the liquid phase (L_α).[1] The enthalpy for the $P_{\beta'} \leftrightarrow L_\alpha$ phase transition has the highest value because of the major structural changes in the aliphatic interior of the bilayer.[1,23] The $P_{\beta'} \leftrightarrow L_\alpha$ transition occurs at ~23 °C for DMPC lipids (~42 °C for DPPC).[1,23] Porphyrin **1** fluorescence emission intensity increases by about 12% when the phospholipid bilayer undergoes $P_{\beta'} \leftrightarrow L_\alpha$ phase transition (Figure 1B). A well-defined phase transition temperature (~23 °C) observed in the fluorescence emission data indicates that porphyrins **1** are localized in the aliphatic interior of the membrane.[9] (Porphyrins that localize at the membrane surface have different fluorescence emission temperature dependence.[8−12]) Within accuracy of the experiments, the same $P_{\beta'} \leftrightarrow L_\alpha$ phase transition temperature was obtained in differential scanning calorimetry experiments on liposomes with and without porphyrins. This result suggests that porphyrin sensitizers do not significantly perturb the phospholipid bilayer.

Additional information about porphyrin localization in the phospholipid bilayers can be obtained from fluorescence emission quenching studies.[8−12] For these experiments, different amounts of KI were added to liposome solutions while keeping the ionic strength of the solution constant with KCl (0.1 mM $Na_2S_2O_3$ was also used to prevent oxidation of I^-). At higher iodide concentration, the porphyrin fluorescence emission yield

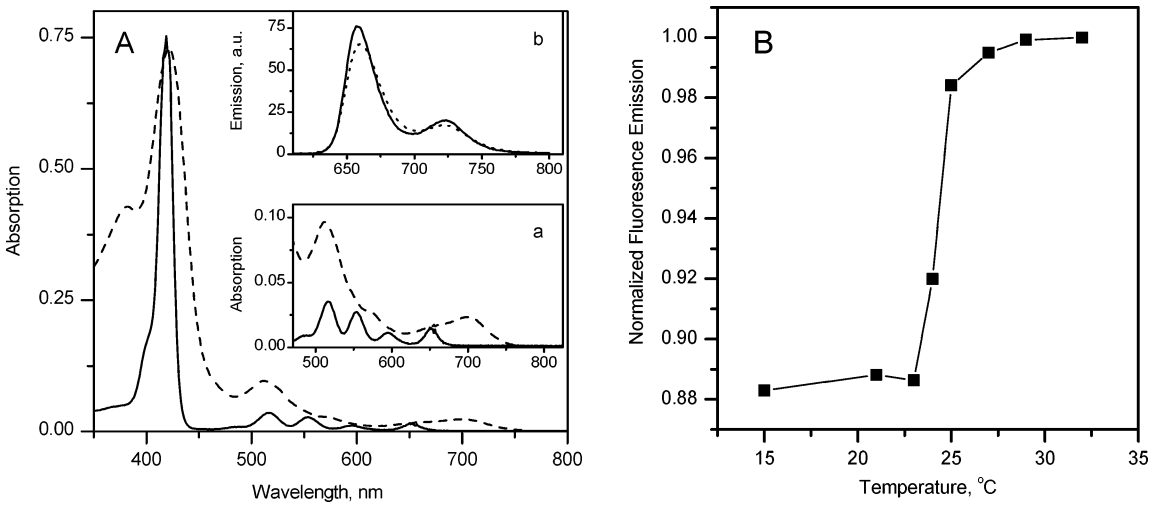

Figure 1. A. Electronic absorption spectra for porphyrins **1** (—) and **2** (- - -) in acetone solution. Inset a: Expansion of the porphyrin Q-band region in the absorption spectrum. Inset b: Porphyrin **1** fluorescence emission spectra in acetone solution (—) and embedded in liposomes (···· ····). B. Fluorescence emission intensity temperature dependence for **1**/DMPC liposomes. Phospholipid/porphyrin ratio was 1000:1, excitation wavelength was 550 nm. The data were obtained by integrating fluorescence emission between 620 and 760 nm. **1**/DMPC absorption and emission spectra do not change in this temperature range.

was lower due to excited-state quenching by iodide. Analysis of the quenching data according to a Stern−Volmer model yields the excited-state quenching rate.[25] A modified Stern−Volmer model was used because a simple Stern−Volmer model was not consistent with the data. The modified Stern−Volmer model is based on the assumption that there are two-distinct groups of porphyrins, one group that is quenched efficiently and the other group that is quenched slower. The difference between the two groups could be their depth in the phospholipid bilayer. While several porphyrins embedded in phospholipid bilayers were extensively investigated (because of their potential as anticancer agents),[8−12] hydroxyphenyl porphyrin embedding depth has not been determined conclusively. Therefore, a more complex distribution, such as the presence of more than two distinct populations or a continuous depth distribution, cannot be excluded. We are primarily interested in whether the porphyrin distribution in the liposome membrane (embedding depth) is the same in L_{β}' and L_{α} phases of the membrane. To answer this question, Stern-Vormer analysis is sufficient.

A modified Stern−Volmer plot of **1**/DPPC fluorescence emission intensity versus the inverse of iodide concentration is shown in Figure 2. Two data sets were collected, at 25 °C (L_{β}' phase of the bilayer) and at 55 °C (L_{α} phase). Fluorescence intensity, F, was analyzed as[25]

$$\frac{F_0}{\Delta F} = \frac{1}{f_a K_a [KI]} + \frac{1}{f_a} \qquad (2)$$

where F_0 is fluorescence intensity without quencher, $\Delta F = F_0 - F$, f_a is the fraction of porphyrin molecules which are accessible to the quencher, K_a is the Stern−Volmer quenching constant of the accessible fraction, and [*KI*] is the concentration of the quencher. Fitting of the data yields similar f_a values at both temperatures, $f_a = 0.78$ (25 °C) and 0.81 (55 °C); therefore, the fraction of the porphyrin molecules exposed to the quencher does not change significantly in gel and liquid crystal phases of the membrane. Based on this result, we assume that porphyrin localization does not change in different phases of the bilayer. The Stern−Volmer constant is somewhat larger at 55 °C, $K_a = 6.8\ M^{-1}$, than at 25 °C, $K_a = 5.9\ M^{-1}$. The Stern−Volmer constant for quenching with iodide has values similar to those

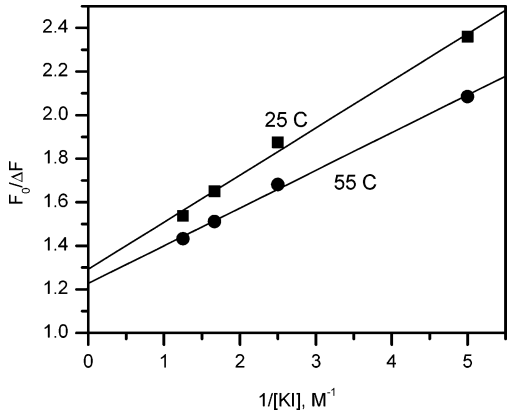

Figure 2. Modified Stern−Volmer plot of **1**/DPPC fluorescence emission quenching with iodide. [*KI*] concentration is varied from 0 to 0.80 M. Phospholipid/porphyrin ratio was 1000:1. Excitation was at 550 nm; integrated emission was measured at 620−760 nm. Temperature was 25 °C (■) and 55 °C (●). Solid lines were obtained by fitting data to eq 2.

determined for other porphyrins, especially those that localize in the aliphatic region of the bilayer.[8]

Photophysical characteristics of **1** in phospholipid bilayers can be contrasted to those of carboxylic porphyrins (such as hematoporphyrin).[8,10] In DMPC and DPPC liposomes, carboxylic porphyrin emission intensity *decreases* at higher temperatures; porphyrin distribution between various compartments of the membrane and aggregation behavior are also influenced by temperature changes.[8,10] This does not appear to be the case for porphyrin **1**.

Transient Grating Kinetics for Aqueous Solutions of Porphyrin 3. Transient grating kinetics for porphyrin **3** aqueous solution are shown in Figure 3. Temperatures at which data were collected are indicated on the graph. Within the accuracy of the experiment, dynamics at $t < 3$ ps are indistinguishable. The peak at $t = 0$ ps (when excitation and probe pulses overlap in time) is assigned to the Optical Kerr effect. The width of this peak (fwhm = 0.40 ps) is somewhat larger than fwhm of the laser pulses used for excitation; this broadening is observed because of the relatively large angle between the excitation pulses ($\Theta = 13.6°$, Scheme 2). Both resonant and nonresonant effects contribute to the femtosecond Optical Kerr effect signal.

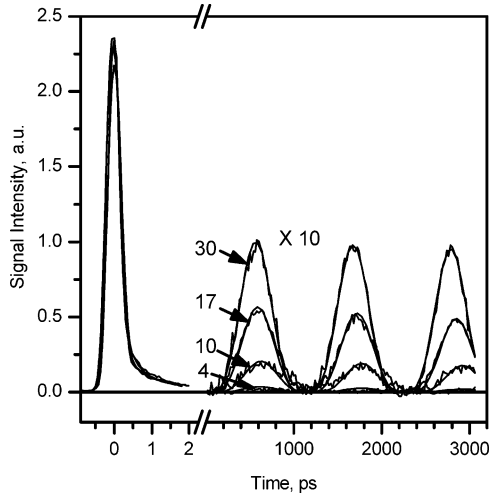

Figure 3. Porphyrin **3** aqueous solution (phosphate buffer, pH 7) transient grating kinetics measured at 30, 17, 10, and 4 °C (amplitudes from the highest to the lowest). Note different scale used for time axis. For clarity, all signals at 20−3000 ps time delay were multiplied ×10. Solid lines are fits according to eq 3.

The resonant contribution arises due to the iron porphyrin excited-state absorption at the probe wavelength of 820 nm,[26] while nonresonant contributions are related to the nonlinear polarizability of the hydroxyphenyl porphyrin macrocycle.[27]

A small amplitude picosecond decay component is also evident at 0.5−3 ps time delay in Figure 3. Assuming an exponential decay, the lifetime of this component is 1.5 ps. The amplitude is the same at all temperatures. Because the grating response is quadratic in time (see eq 1), the apparent 1.5 ps decay corresponds to 3 ps relaxation of the porphyrin exited states. Similar ps relaxation components observed for iron porphyrins were attributed to electronic and vibrational relaxation.[28−30] For example, anti-Stokes band ν_4 (which corresponds to 1375 cm^{-1} macrocycle skeletal vibrations) for **3** had a 1.9 ps lifetime in water.[30] Based on the analysis of the Optical Kerr effect signal, we conclude that the electronic excited states for porphyrin **3** relax within several picoseconds.

Next we analyze the oscillating signal at 20−3000 ps in Figure 3. At 4 °C, when the water volume thermal expansion coefficient, β_W, is equal to zero, the amplitude of the oscillating signal is negligible. Signal amplitude increases at higher temperatures concomitant with an increase in β_W. Therefore, the oscillating part of the kinetics is assigned to the acoustic signal (see methods section) in aqueous solution. A nonlinear least squares Levenberg−Marquardt algorithm was used to fit the acoustic data (measured at 20−3000 ps time delay) to the following function (α is the grating decay rate constant):

$$I_{\text{grating}} = A\left(\sin\frac{2\pi(t - t_c)}{\Pi}\right)^2 \exp(-\alpha t) \qquad (3)$$

Fitting results are shown as solid lines in Figure 3; *A*, Π, and t_c values at different temperatures are summarized in Figure 5 A−C. The exponential term in eq 3 describes the transient grating decay; $\alpha \approx 1 \times 10^8$ s^{-1}. The rate constant α provides detailed information about the microscopic viscosity.[31] Our experiments were limited to a 3 ns time scale. Analyzing longer time kinetics would yield more reliable α values. Period Π data (Figure 5B) simply reflect the temperature dependence of the speed of sound, *c*, in aqueous solution ($c = \Lambda/\Pi = 1.55 \times 10^3$ m s^{-1} at 25 °C; literature value for *c* in water at this temperature is 1.50×10^3 m s^{-1}).[32]

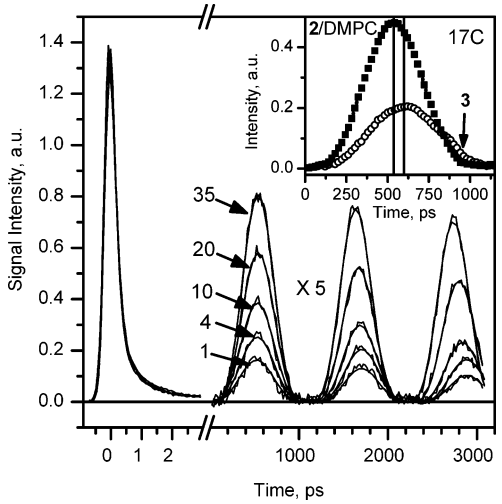

Figure 4. Transient grating kinetics for **2**/DMPC liposomes measured at 35, 20, 10, 4, and 1 °C (amplitudes from the highest to the lowest). Note different scale used for time axis. For clarity, all signals at 20−3000 ps time delay were multiplied ×5. Solid lines represent fits according to eq 3. Inset: expansion of 17 °C acoustic signals at 20−1100 ps for **2**/DMPC liposomes (−■−) and for **3** aqueous solution (−○−). Kinetics differ in amplitude and in acoustic peak delay.

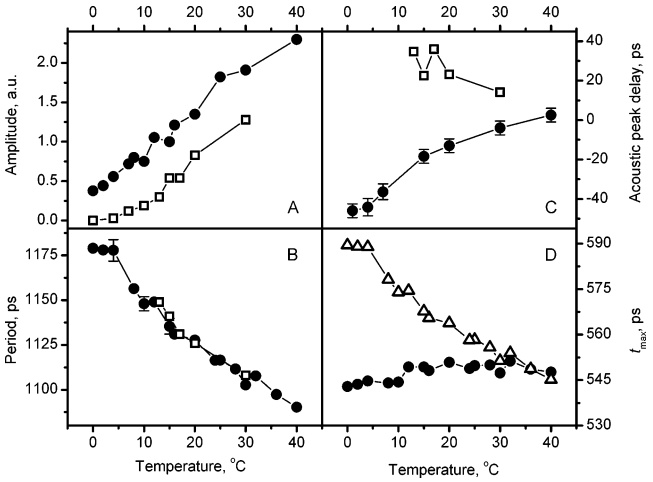

Figure 5. Amplitude *A* (A), period Π (B), and acoustic peak delay t_c (C) temperature dependence determined by fitting data to eq 3. Parameters are shown for **2**/DMPC liposomes (−●−) and for **3** aqueous solution (−□−). D Experimentally determined time when the first acoustic peak reaches its maximum for **2**/DMPC liposomes (−●−); this time equals $\Pi/2 + t_c$. In the case of instantaneous thermal relaxation and volume expansion, t_{max} would be observed at Π/2 (−△−).

The most important results were obtained from the amplitude, *A*, and the acoustic peak delay, t_c, temperature dependence data. Figure 5C shows that t_c varies between 20 and 30 ps (small TG signal amplitude precluded reliable t_c determination below 10 °C). Following the analysis of Terazima and co-workers,[17,33,34] t_c data are assigned to porphyrin thermalization with $\tau \approx 25$ ps. Because electronic excited-state relaxation for **3** is significantly faster than 25 ps, thermalization with $\tau \approx 25$ ps reflects vibrational energy transfer from the porphyrin electronic ground state to water.

Transient Grating Kinetics for 2/DMPC Liposomes. Transient grating kinetics measured for **2**/DMPC liposomes at several temperatures are shown in Figure 4. Assignment of the $t = 0$ ps peak to the Optical Kerr effect and ∼1.5 ps relaxation component to the electronic and vibrational relaxation (with 3 ps lifetime) is the same as for **3** aqueous solution.

Oscillating (acoustic) signals at 20−3000 ps for **2**/DMPC liposomes were also fitted to eq 3; parameters are summarized in Figure 5 A−C (grating decay rate constant $\alpha \approx 1 \times 10^8$ s^{-1}). Period Π values (B) appear to be the same as for **3** aqueous solution, while amplitude, *A*, (A) and acoustic peak delay, t_c, (C) values are different. The main differences are: (1) acoustic signals for **2**/DMPC liposomes have larger amplitude; (2) **2**/DMPC liposome signal amplitude is significant at 4 °C, when the water thermal expansion coefficient is zero and **3** aqueous solution signal amplitude is negligible; and (3) the phase shift for **2**/DMPC acoustic signals is *negative* ($t_c < 0$) and strongly temperature-dependent.

The larger amplitude for **2**/DMPC liposome transient grating signals is attributed to liposome thermal expansion. The volume thermal expansion coefficient for lipids, β_L, has similar values in both gel ($\beta_L = 0.00088$ K^{-1}) and liquid ($\beta_L = 0.001$ K^{-1}) phases of the bilayer.[23,35] In contrast, the volume thermal expansion coefficient for water, β_W, changes nonlinearly with temperature.[32] The difference between β_L and β_W values is greatest at 4 °C, when $\beta_W = 0$.

The negative phase shift ($t_c < 0$) is particularly interesting. As described in the Methods section, a finite relaxation rate in systems described by a single thermalization rate constant could only result in *positive* acoustic peak delays, $t_c > 0$. A positive acoustic peak delay was observed for **3** aqueous solution at 12−30 °C (Figure 5C). The inset in Figure 4 contrasts 17 °C kinetics for **3** aqueous solution and for **2**/DMPC liposomes. Clearly, acoustic signals for **2**/DMPC liposomes reach maximal values at earlier times, which results in $t_c < 0$. Below we develop a model to explain the negative acoustic peak delays by accounting for two steps of porphyrin thermalization in phospholipid bilayers—energy transfer to the membrane followed by energy transfer to the surrounding solvent (Scheme 1). Interference of the acoustic waves created by the two processes causes the apparent negative acoustic peak delay.

Finally, Figure 5D shows the experimentally determined time of the first acoustic peak maximum for **2**/DMPC liposomes (−●−; also see Scheme 2). Surprisingly, t_{max} does not vary with temperature when the acoustic period changes; the increase in $\Pi/2$ at low temperatures is compensated by a negative phase shift, and $t_{max} = \Pi/2 + t_c \approx 545$ ps.

Discussion

Thermal Relaxation Dynamics and Volume Expansion. Following excitation at 410 nm, 3.02 eV (or 291 kJ mol^{-1}) excess energy is absorbed by the porphyrins. This energy is dissipated in electronic and vibrational degrees of freedom.[36] Electronic excited-state relaxation is reflected in the Optical Kerr effect signals in Figures 3 and 4 (kinetics at time delay < 3 ps). As explained in Results, electronic relaxation can be approximated with fs and 3 ps lifetime components. For **2**/DMPC liposomes, porphyrin electronic excited-state relaxation is followed by a vibrational energy transfer to the phospholipid bilayer. (Based on fluorescence emission temperature dependence studies, we assume that there is no direct energy transfer from porphyrin **2** to water). The upper limit for the increase in liposome temperature is 1.4 K (50-nm-diameter liposomes consist of ~20 000 phospholipids, heat capacity of DMPC phospholipid bilayer is 1600 J mol^{-1} K^{-1},[23] ~150 porphyrins are excited in one **2**/DMPC liposome based on sample absorbance of 0.65 and 100:1 lipid/porphyrin ratio). An increase in the liposome temperature leads to the thermal expansion.

Porphyrins embedded in the lipid bilayers (**2**/DMPC) can perhaps be compared to the heme in deoxymyoglobin. Li and Champion modeled thermal processes in deoxymyoglobin by considering the thermal response of an instantaneously heated chromophore embedded in a protein and surrounded by water.[37] The temperature for such a system (obtained by numerically solving a two-boundary thermal transport problem) was well-approximated by a two-exponential function (in a longer time limit solutions "rolled over" to a $t^{-3/2}$ decay with a very small amplitude).[37] Similarly, cooling of deoxymyoglobin heme in transient mid-IR absorption experiments was modeled by an exponential decay with a time constant τ of 3−10 ps.[38] Thermalization of dye molecules in various organic solvents was also assumed to be exponential.[39] Therefore, an exponential function is a satisfactory first-order approximation for thermal relaxation of photoexcited porphyrins (experimental data do not justify a more complex model, such as including a second exponent or a $\sim t^{-3/2}$ component):

$$Q_P = Q \exp(-k_1 t) \tag{4}$$

where k_1 is a first-order rate constant that describes porphyrin thermalization, Q_P is porphyrin excess energy (heat), and Q is total excess energy. Similarly, excess heat in liposomes and in water is described as

$$Q_L = \frac{Qk_1}{k_2 - k_1}\{\exp(-k_1 t) - \exp(-k_2 t)\} \tag{5}$$

$$Q_W = Q - Q_P - Q_L = \left(1 + \frac{k_1 \exp(-k_2 t) - k_2 \exp(-k_1 t)}{k_2 - k_1}\right)Q \tag{6}$$

where k_2 is a first-order rate constant that describes liposome thermalization (Scheme 1), and Q_L and Q_W are excess energies for liposomes and water, respectively. Deposition of excess heat causes volume thermal expansion corresponding to liposome expansion, $dV_L(t)$, and water expansion, $dV_W(t)$

$$dV = dV_L(t) + dV_W(t) = \frac{\beta_L dQ_L}{\rho_0 C_{PL}} + \frac{\beta_W dQ_W}{\rho_0 C_{PW}} \tag{7}$$

where ρ_0 is density, β_L and β_W are the volume expansion coefficients for phospholipid bilayers and water ($\beta = V^{-1}(\partial V/\partial T)_P$), C_{PL} and C_{PW} are heat capacities for phospholipid bilayers and water, respectively ($C_P = (\partial H/\partial T)_P \approx dQ/dT$).

Model for Transient Grating Data taking into account Time Dependence of Phospholipid Bilayer and Solvent Thermal Expansion. Chen and Diebolt derived an analytical expression for describing the temporal profile of an acoustic wave created by thermal expansion in solution.[40] Puchenkov and Malkin considered pulse-width effect on the rise time of the transient grating kinetics.[41] Deàk et al. modified this model to include time-dependent structural relaxation.[20] We also start with the models of Puchenkov and Malkin[41] and Deàk et al.[20] but consider time-dependent thermal expansion. The wave equation describing density modulation, $\delta(t,x) = \rho(t) - \rho_0$, due to liposome and solvent thermal expansion is[20,41]

$$\frac{\partial^2 \delta(t,x)}{\partial x^2} - \frac{1}{c^2}\frac{\partial^2 \delta(t,x)}{\partial t^2} = \frac{\rho_0}{c^2}\frac{\partial^2 V}{\partial t^2} \tag{8}$$

Substitution, $\delta(t,x) = D(t)\sin(2\pi x/\Lambda)$, is used to separate temporal and spatial variables; $D(t)$ describes maximal density changes for the grating. The time dependence for $D(t)$ is represented by

$$\frac{d^2D(t)}{dt^2} + \omega^2 D(t) = -\rho_0 \frac{d^2V}{dt^2} \quad (9)$$

The second derivative for $V(t)$ is obtained from eqs 5−7. Substituting this result into eq 9 yields

$$\frac{d^2D(t)}{dt^2} + \omega^2 D(t) = -\frac{Qk_1^2}{k_2 - k_1}\left(\frac{\beta_L}{C_{PL}}k_1 - \frac{\beta_W}{C_{PW}}k_2\right)\exp(-k_1 t) - \frac{Qk_1k_2^2}{k_2 - k_1}\left(\frac{\beta_L}{C_{PL}} - \frac{\beta_W}{C_{PW}}\right)\exp(-k_2 t) \quad (10)$$

Equation 10 can be solved analytically using the initial conditions $D(0) = 0$ and $D'(0) = 0$ (i.e., no density perturbations at $t = 0$). The solution comprises three terms: exponential relaxation, sin(wt), and cos(wt) acoustic waves

$$D(t) = A_1 \exp(-k_1 t) + A_2 \exp(-k_2 t) + A_3 \sin(wt) + A_4 \cos(wt) \quad (11)$$

where coefficients are

$$A_1 = \frac{Qk_1^2(\beta_W C_{PL} k_2 - \beta_L C_{PW} k_1)}{C_{PL}C_{PW}(k_2 - k_1)(k_1^2 + w^2)}$$

$$A_2 = \frac{Qk_1k_2^2(\beta_L C_{PW} - \beta_W C_{PL})}{C_{PL}C_{PW}(k_1 - k_2)(k_2^2 + w^2)}$$

$$A_3 = [\{Qk_1\beta_L C_{PW}(k_1^3k_2^2 + k_1^2k_2^3 + k_1^3w^2 + k_2^3w^2)\} - \{\beta_W C_{PL}k_2(2k_1^2k_2^2 + k_1^2w^2 + k_2^2w^2)\}]/[C_{PL}C_{PW}(k_1 - k_2)(k_1^2 + w^2)(k_2^2 + w^2)w]$$

$$A_4 = [\{Qk_1 - \beta_L C_{PW}(2k_1^2k_2^2 + k_1^2w^2 + k_2^2w^2)\} + \{\beta_W C_{PL}k_2(k_1 + k_2)(k_1k_2 + w^2)\}]/[C_{PL}C_{PW}(k_1 - k_2)(k_1^2 + w^2)(k_2^2 + w^2)]$$

The physical significance of the two oscillating terms, $A_3\sin(wt)$ and $A_4\cos(wt)$, becomes clear from the analysis of the thermal expansion process of this complex system. The $A_3\sin(wt)$ term is related to the total volume expansion due to liposome heating. The $A_4\cos(wt)$ term is related to a decrease in the total volume due to heat transfer to the aqueous solvent. Comparison with the data shows that the $A_3\sin(wt)$ amplitude is greater, but the $A_4\cos(wt)$ contribution determines acoustic peak shift t_c values.

Finally, $[D(t)]^2$ can be compared to the experimental data, $I_{grating}$ (see eq 1)

$$I_{grating} \propto \left(\frac{\partial n}{\partial \rho}\right)_T^2 \delta^2(t) = \left(\frac{\partial n}{\partial \rho}\right)_T^2 \left[D(t)\sin\left(\frac{2\pi x}{\Lambda}\right)\right]^2 \quad (12)$$

The term due to temperature change ($(\partial n/\partial T)_\rho dT$ of eq 1) is not included in eq 12. In general, the phases of the thermal and acoustic terms are different—thermal contributions appear following electronic and vibrational relaxation, while density changes evolve with acoustic wave propagation.[20] Negligible transient grating signal amplitudes at $t \approx 20$, $t \approx 1100$, and $t \approx 2200$ ps suggest that only density changes are important and therefore only the acoustic grating is considered.

Modeling Results. Equations 11 and 12 were used to model **2**/DMPC transient grating kinetics measured at different temperatures. While eq 11 is complex, there are only two adjustable parameters: rate constants k_1 and k_2. Other parameters used for fitting were obtained from the literature: $C_{PL} = 1600$ J mol^{-1} K^{-1},[23] $C_{PW} = 75.3$ J mol^{-1} K^{-1},[32] $\beta_L = 8.8 \times 10^{-4}$ K^{-1}.[23] The water volume thermal expansion coefficient, β_W, was calculated as $\beta_W = V_W^{-1}(\partial V_W/\partial T)_P$, and the cubic approximation for the water volume temperature dependence was used: $V_W = V_{0W}(1 - 6.427 \times 10^{-5}\,\check{T} + 8.5053 \times 10^{-6}\,\check{T}^2 - 6.7900 \times 10^{-8}\check{T}^3)$, where $\check{T}$ is temperature expressed in °C.[42] Frequency w temperature dependence was obtained from the grating period data (Figure 5B). Linear approximation yielded $w = 0.00267 + 5.6 \times 10^{-6}\,\check{T}$.

Figure 6 shows experimental and simulated **2**/DMPC liposome acoustic signals at 10 °C (A) and 24 °C (B). At 10 °C, two simulated kinetics are shown. Simulation with $k_1 = 1.0 \times 10^{12}$ s^{-1} and $k_2 = 3.33 \times 10^{10}$ s^{-1} ($t_{max} = 576$ ps) does not fit the data, while simulation with $k_1 = 7.14 \times 10^{10}$ s^{-1} and $k_2 = 3.33 \times 10^{10}$ s^{-1} ($t_{max} = 546$ ps) is in agreement with the experimental results. As evident from the two simulations shown, *slower* energy transfer from porphyrin to the phospholipid bilayer results in an *earlier* t_{max} time of the acoustic wave—and therefore negative t_c values. As explained above, this effect is caused by the interference of the two acoustic waves created due to liposome and aqueous solution thermal expansion. As shown in Figure 6B, 24 °C data can be simulated using the same porphyrin thermalization rate constant, $k_1 = 7.14 \times 10^{10}$ s^{-1}, but the rate constant k_2 is somewhat larger, $k_2 = 4.35 \times 10^{10}$ s^{-1} ($t_{max} = 545$ ps). The model is sensitive to the variations in the rate constant values. For example, simulation with $k_1 = 7.14 \times 10^{10}$ s^{-1} and $k_2 = 3.33 \times 10^{10}$ s^{-1} does not fit the data in Figure 6B ($t_{max} = 477$ ps).

Figure 7 summarizes the temperature dependence of rate constants k_1 and k_2 determined from simulations. At higher temperatures (≥10 °C) $k_1 = 7.14 \times 10^{10}$ s^{-1} ($k_1^{-1} = 14$ ps), while at 4 and 8 °C k_1 values are lower. Rate constant k_1 describes vibrational energy transfer from Fe(III) porphyrins to the phospholipid bilayer. Below 13 °C, DMPC bilayers are in the highly ordered $L_{\beta'}$ phase. Different interaction between the porphyrin and the phospholipid alkyl chains might explain lower k_1 values in the $L_{\beta'}$ phase. Rate constant k_1 values are in good agreement with the heme thermalization rate constants determined in MD simulations,[43,44] transient absorption,[36,38,45] time-resolved Raman,[30,46] and transient grating[47] experiments. Similar electronic and vibrational relaxation rate constants were also reported for iron porphyrins in solution.[28−30]

Rate constant k_2 describes vibrational energy transfer from phospholipid bilayers to water. k_2 is temperature-dependent and ranges between $k_2^{-1} = 50$ ps (at 4 °C) to $k_2^{-1} = 18$ ps (at 35 °C). Determination of k_2 is significant because this information cannot be obtained from experiments that only study linear spectroscopic properties of membrane-embedded molecular probes. Extension of transient grating studies to other phospholipid bilayer membranes, which differ in thickness or charge distribution, could provide new information about the physical characteristics of biological membranes. Until now, phospholipid bilayer interaction with water on ps time scale could only be studied in MD simulations.

Analysis of Thermalization in Membranes and Comparison with Other Studies. The DMPC bilayer thickness is 4.8 nm in the gel phase ($L_{\beta'}$) and 3.9 nm in the liquid (L_α) phase,[1,23] therefore the distance through which excess energy is transferred is about 2 nm (assuming that porphyrins are localized in the aliphatic region of the bilayer as suggested by fluorescence studies). Two estimates can be made for the rates of vibrational

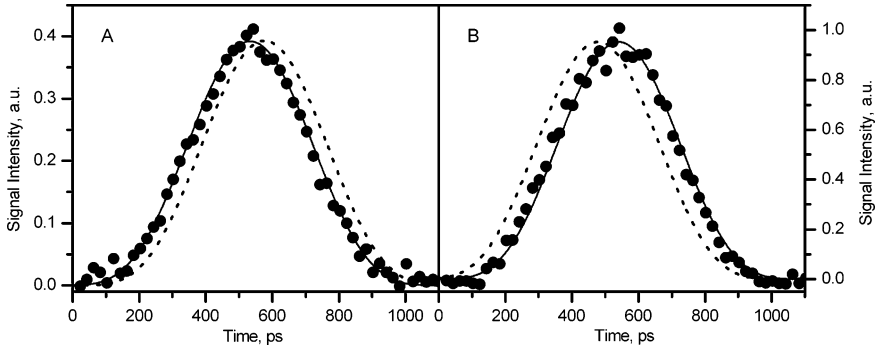

Figure 6. Simulation of **2**/DMPC liposome transient grating data (●) measured at 10 °C (A) and at 24 °C (B). The following rate constants were used in simulations according to eqs 11 and 12: (A) $k_1 = 1.0 \times 10^{12}$ s^{-1}, $k_2 = 3.33 \times 10^{10}$ s^{-1} (- - -) and $k_1 = 7.14 \times 10^{10}$ s^{-1}, $k_2 = 3.33 \times 10^{10}$ s^{-1} (—); (B) $k_1 = 7.14 \times 10^{10}$ s^{-1}, $k_2 = 3.33 \times 10^{10}$ s^{-1} (- - -) and $k_1 = 7.14 \times 10^{10}$ s^{-1}, $k_2 = 4.35 \times 10^{10}$ s^{-1} (—).

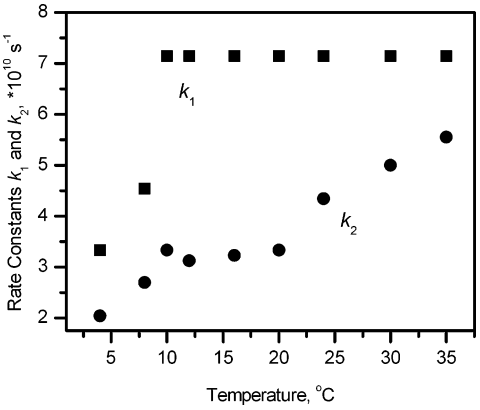

Figure 7. Temperature dependence of rate constants k_1 (■) and k_2 (●) for **2**/DMPC liposomes. Rate constants were determined by simulating transient grating data (Figure 4) with eqs 11 and 12.

energy transfer from the membrane aliphatic interior to the surrounding water. First, the thermal diffusivity in proteins (such as the photosynthetic reaction center and myoglobin) is $D_T = 7-14$ Å^2/ps.[48,49] The time required for energy transfer across the distance $L = 2$ nm in a system with such diffusivity is $t_D = L^2/(2\ D_T) = 28-56$ ps. Second, the rate of vibrational energy transfer along the alkyl backbone has been directly examined; the time for vibrational energy transfer increased by about 0.4 ps per CH_2 group.[50] DMPC fatty acid residues have 13 CH_2 groups, so estimated energy transfer time through such fatty acid residue is 5.2 ps. The first estimate is in better agreement with experimentally measured k_2 values. This suggests that energy transfer through the phospholipid bilayer predominantly occurs by thermal diffusion. In the liquid phase of the membrane (L_α), phospholipid fatty acid chains adopt various conformations. While disordered, they remain in van der Waals contact. Such conformational disorder may explain diffusion-like vibrational energy transfer in liquid-phase membranes. Decrease in k_2 values in the ordered bilayer phases could be the result of an increase in bilayer thickness.

While rate constant k_2 increases from 2.0×10^{10} s^{-1} to 5.6×10^{10} s^{-1} when the temperature changes from 4 to 35 °C, the change appears monotonic and no discontinuity is observed at the phase transition temperatures (13 and 23 °C for DMPC lipids). This is unexpected, since many physical characteristics of the membrane change during these transitions.[1]

Different results were obtained with acoustic spectroscopy.[51−53] In these experiments, phospholipid bilayer relaxation times were obtained from modeling ultrasonic excess attenuation spectra measured at frequencies up to 2 GHz.[51−53] Close to the main phase transition ($P_{\beta'} \leftrightarrow L_\alpha$), ns and μs relaxation times become significantly longer. These relaxation times were assigned to isomerization of the fatty acid residues and density fluctuations in the bilayer.[52,53] In our time-domain experiments, the acoustic period varied between 1080 and 1180 ps (Figure 5B), which in frequency domain correspond to 0.85−0.93 GHz—but by analyzing acoustic peak shifts, we examined much higher frequency dynamics, which could explain the difference from broadband acoustic spectroscopy results.

Other experiments examined ultrasonic velocity at a single acoustic frequency (at <10 MHz).[54,55] Such ultrasonic velocity had discontinuity close to the main phase transition temperature. Unlike these results, our investigations showed that the speed of sound in 0.85−0.93 GHz frequency domain has no discontinuity at the $P_{\beta'} \leftrightarrow L_\alpha$ phase transition temperature. Much higher frequency dynamics examined in transient grating experiments could explain this difference as well.

Phospholipid dynamics in membranes consists of a wide range of motions that span many different time scales—from 10^{-14} s for vibrations to hours for transbilayer exchange of lipid molecules. Only vibrations, torsional oscillations, and trans-gauche isomerizations occur on the subnanosecond time scale. Other motions are slower.[1] While bilayer properties are very different in L_α, $P_{\beta'}$, and $L_{\beta'}$ phases, correlation times for vibrations, torsional oscillations, and isomerization do not differ significantly.[1] The insensitivity of k_2 to the phase of the bilayers suggests that, following excitation with short laser pulses, energy relaxation in the phospholipid bilayer membrane happens through vibrational energy transfer, but phospholipid isomerization and other large scale motions are not excited.

Conclusions

In summary, we have examined ultrafast thermal processes in phospholipid bilayer liposomes with embedded porphyrin sensitizers. Use of transient grating nonlinear optical spectroscopy allowed us to study energy transfer from molecular sensitizers to phospholipid bilayers as well as energy transfer from phospholipid bilayers to water. Modeling of the transient grating acoustic peak delay data was used to obtain rate constants that describe these processes. We find that porphyrin electronic and vibrational relaxation in phospholipid bilayers occurs with rate constants similar to those found in organic solvents, $k_1 = 3-7 \times 10^{10}$ s^{-1}. Picosecond thermal energy transfer from phospholipid bilayers to water has a weak temperature dependence and occurs with similar rates in gel and liquid phases of the bilayer.

Acknowledgment. We thank Dr. Rick van Antwerpen of VCU Department of Biochemistry for help with DSC measure-

ments. D.K. acknowledges generous support from VCU, and partial support of this research by the Jeffress Memorial Trust.

References and Notes

(1) Cevc, G., Ed. *Phospholipids Handbook*; Marcel Dekker: New York, 1993.
(2) Fendler, J. H. *Membrane-Mimetic Approach to Advanced Materials*; Springer-Verlag: Berlin, 1994.
(3) Gust, D.; Moore, T. A.; Moore, A. L. *Acc. Chem. Res.* **2001**, *34*, 40.
(4) Bonnett, R. *Chem. Soc. Rev.* **1995**, *24*, 19.
(5) Bonnett, R.; McGarvey, D. J.; Harriman, A.; Land, E. J.; Truscott, T. G.; Winfield, U. J. *Photochem. Photobiol.* **1988**, *48*, 271.
(6) Bonnett, R.; Charlesworth, P.; Djelal, B. D.; Foley, S.; McGarvey, D. J.; Truscott, T. G. *J. Chem. Soc. Perkin. Trans. 2* **1999**, 325.
(7) Bonnett, R.; White, R. D.; Winfield, U. J.; Berenbaum, M. C. *Biochem. J.* **1989**, *261*, 277.
(8) Ricchelli, F.; Jori, G. *Photochem. Photobiol.* **1986**, *44*, 151.
(9) Redmond, R. W.; Valduga, G.; Nonell, S.; Braslavsky, S. E.; Schaffner, K. *J. Photochem. Photobiol.* **1989**, *3*.
(10) Ricchelli, F. *J. Photochem. Photobiol., B* **1995**, *29*, 109.
(11) Vermathen, M.; Louie, E. A.; Chodosh, A. B.; Ried, S.; Simonis, U. *Langmuir* **2000**, *16*, 210.
(12) Lavi, A.; Weitman, H.; Holmes, R. T.; Smith, K. M.; Ehrenberg, B. *Biophys. J.* **2002**, *82*, 2101.
(13) Ishikawa, Y.; Kunitake, T. *J. Am. Chem. Soc.* **1991**, *113*, 621.
(14) Genberg, L.; Richard, L.; McLendon, G.; Miller, R. J. D. *Science* **1991**, *251*, 1051.
(15) Harata, A.; Shen, Q.; Sawada, T. *Annu. Rev. Phys. Chem.* **1999**, *50*, 193.
(16) Terazima, M. In *Advances in Photochemistry, Volume 24*; Neckers, D. C., Volman, D. H., Eds.; John Wiley & Sons: New York, 1998.
(17) Okazaki, T.; Hirota, N.; Terazima, M. *J. Chem. Phys.* **1999**, *110*, 11399.
(18) Terazima, M.; Takezaki, M.; Yamaguchi, S.; Hirota, N. *J. Chem. Phys.* **1998**, *109*, 603.
(19) Miyata, R.; Terazima, M. *Bull. Chem. Soc. Jpn.* **2003**, *76*, 1707.
(20) Deàk, J.; Chin, H. L.; Lewis, C. M.; Miller, R. J. D. *J. Phys. Chem. B* **1998**, *102*, 6621.
(21) Terazima, M. *Chem. Phys.* **1994**, *189*, 793.
(22) Okazaki, T.; Hirota, N.; Terazima, M. *J. Phys. Chem. A* **1997**, *101*, 650.
(23) Heimburg, T. *Biochim. Biophys. Acta* **1998**, *1415*, 147.
(24) Kuciauskas, D.; Porsch, M. J.; Pakalnis, S.; Lott, K. M.; Wright, M. E. *J. Phys. Chem. B* **2003**, *107*, 1559.
(25) Lakowicz, J. R. *Principles of Fluorescence Spectroscopy, 2nd ed.;* Kluwer Academic/Plenum Publishers: New York, 1999.
(26) Rodriguez, J.; Kirmaier, C.; Holten, D. *J. Am. Chem. Soc.* **1989**, *111*, 6500.
(27) Humphrey, J.; Kuciauskas, D. *J. Phys. Chem. B* **2004**, *108*, 12016.
(28) Dixon, D. W.; Kirmaier, C.; Holten, D. *J. Am. Chem. Soc.* **1985**, *107*, 808.
(29) Cornelius, P. A.; Steele, A. W.; Chernoff, D. A.; Hochstrasser, R. M. *Chem. Phys. Lett.* **1981**, *82*, 9.
(30) Mizutani, Y.; Kitagawa, T. *Bull. Chem. Soc. Jpn.* **2002**, *75*, 623.
(31) El-Sayed, M. Y.; Guion, T. A.; Fayer, M. D. *Biochemistry* **1986**, *25*, 4825.
(32) Lide, D. R., Ed. *CRC Handbook of Chemistry and Physics*, 77th ed.; CRC Press: Boca Raton, FL, 1996.
(33) Saga, N.; Kimura, Y.; Hirota, N.; Terazima, M. *Chem. Phys. Lett.* **2000**, *332*, 496.
(34) Terazima, M. *Chem. Phys. Lett.* **1999**, *305*, 189.
(35) Nagle, J. F.; Wilkinson, D. A. *Biophys. J.* **1978**, *23*, 159.
(36) Lim, M.; Jackson, T. A.; Anfinrud, P. A. *J. Phys. Chem.* **1996**, *100*, 12043.
(37) Li, P.; Champion, P. M. *Biophys. J.* **1994**, *66*, 430.
(38) Lian, T.; Locke, B.; Kholodenko, Y.; Hochstrasser, R. M. *J. Phys. Chem.* **1994**, *98*, 11648.
(39) Okazaki, T.; Hirota, N.; Nagata, T.; Osuka, A.; Terazima, M. *J. Phys. Chem. A* **1999**, *103*, 9591.
(40) Chen, H. X.; Diebold, G. J. *J. Chem. Phys.* **1996**, *104*, 6730.
(41) Puchenkov, O. V.; Malkin, S. *Chem. Phys. Lett.* **1996**, *251*, 242.
(42) Perry, R. H.; Green, D. W., Eds. *Perry's Chemical Engineer's Handbook*, 7th ed.; McGraw-Hill: New York, 1997.
(43) Henry, E. R.; Eaton, W. A.; Hochstrasser, R. M. *Proc. Nat. Acad. Sci. U.S.A.* **1986**, *83*, 8982.
(44) Sagnella, D. E.; Straub, J. E. *J. Phys. Chem. B* **2001**, *105*, 7057.
(45) Kholodenko, Y.; Volk, M.; Gooding, E.; Hochstrasser, R. M. *Chem. Phys.* **2000**, *259*, 71.
(46) Mizutani, Y.; Kitagawa, T. *Science* **1997**, *278*, 443.
(47) Miller, R. J. D. *Annu. Rev. Phys. Chem.* **1991**, *42*, 581.
(48) Tesch, M.; Schulten, K. *Chem. Phys. Lett.* **1990**, *169*, 97.
(49) Yu, X.; Leitner, D. M. *J. Phys. Chem. B* **2003**, *107*, 1698.
(50) Wang, Z. H.; Pakoulev, A.; Dlott, D. D. *Science* **2002**, *296*, 2201.
(51) Schrader, W.; Kaatze, U. *J. Phys. Chem. B* **2001**, *105*, 6266.
(52) Halstenberg, S.; Schrader, W.; Das, P.; Bhattacharjee, J. K.; Kaatze, U. *J. Chem. Phys.* **2003**, *118*, 5683.
(53) Schrader, W.; Halstenberg, S.; Behrends, R.; Kaatze, U. *J. Phys. Chem. B* **2003**, *107*, 14457.
(54) Tata, D. B.; Dunn, R. C. *J. Phys. Chem.* **1992**, *96*, 3548.
(55) Schrader, W.; Ebel, H.; Grabitz, P.; Hanke, E.; Heimburg, T.; Hoeckel, M.; Kahle, M.; Wente, F.; Kaatze, U. *J. Phys. Chem. B* **2002**, *106*, 6581.